

Far-Infrared Dielectric Properties of Polar Liquids Probed by Femtosecond Terahertz Pulse Spectroscopy[†]

J. T. Kindt and C. A. Schmuttenmaer*

Department of Chemistry, Yale University, 225 Prospect St., New Haven, Connecticut 06520-8107

Received: January 12, 1996; In Final Form: March 19, 1996[⊗]

We report the frequency-dependent optical constants, $n(\nu)$ and $\alpha(\nu)$, or, equivalently, the complex permittivity $\hat{\epsilon}(\omega) = \epsilon'(\omega) - i\epsilon''(\omega)$, over the frequency range from 2 to 50 cm^{-1} for water, methanol, ethanol, 1-propanol, and liquid ammonia. These spectra have been measured with femtosecond terahertz pulse transmission spectroscopy. These liquids exhibit multiple-Debye behavior, making their frequency-dependent dielectric constants valuable benchmarks for molecular dynamics simulations and other theoretical treatments of liquids.

Introduction

Recently, there has been renewed interest in the spectra of liquids at the low-frequency end ($1\text{--}30\text{ cm}^{-1}$) of the far-infrared (FIR) region of the spectrum. This part of the spectrum is quite important as it falls between the microwave and the FIR regions; the motions that are probed at these frequencies bridge the gap between bulk dielectric relaxation and oscillatory, intermolecular motions. Technical difficulties have prevented extensive study in this region, however.

A relatively new far-infrared light source is provided by femtosecond terahertz (fs THz) pulses.¹ This paper reports the absorption and dispersion spectra of several highly absorbing polar liquids utilizing fs THz pulses. Previous workers have used this technique to study gases,² semiconductors,³ superconductors,⁴ dielectrics,⁵ nonpolar liquids,⁶ and water.⁷ We demonstrate here that transmission spectroscopy with fs THz pulses is an efficient way to obtain the FIR frequency-dependent absorption coefficient and index of refraction of a variety of highly absorbing dipolar liquids in the low-frequency region of the FIR. While this paper focuses on steady state measurements of liquids, it is important to note that these pulses have subpicosecond temporal duration and thereby open the FIR region of the spectrum to direct, time-resolved dynamical studies.⁸

The fs THz pulses are generated by the excitation of charge carriers in a semiconductor material with ultrashort pulses of above-bandgap light.¹ There are several important differences between this type of pulse and conventional pulsed laser sources. The primary difference is that these pulses are approximately $1/2$ optical cycle long. As shown in panel a of Figure 1, the electric field simply rises and falls rather than undergoing many oscillations under a slowly varying intensity envelope, as is the case with pulsed visible lasers. The 3 THz (100 cm^{-1}) bandwidth (Figure 1, panel b) contained in these pulses is equivalent to that in any pulse with similar duration, but in this case its spectral range starts at zero frequency (dc), rather than being centered around a carrier frequency in the visible, infrared, or UV region of the spectrum. This bandwidth provides excellent overlap with the low-frequency, intermolecular spectrum of liquids and is a logical choice for studying liquid motions directly.

One of the most valuable features of these pulses is that it is possible to detect them with an ultrafast antenna receiver and

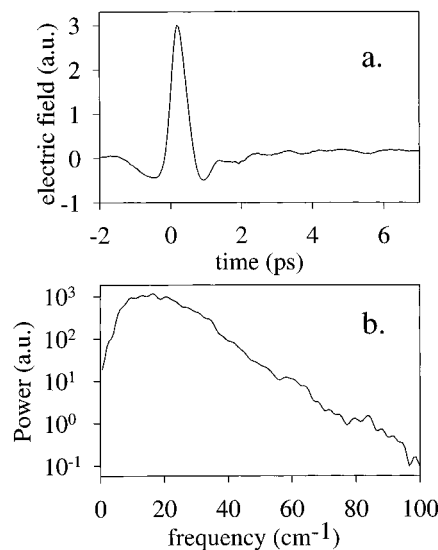


Figure 1. (a) Measured wave form of fs THz pulse, fwhm 600 fs. (b) Power spectrum of the Fourier transform of the pulse shown in (a).

obtain both amplitude and phase information over a wide frequency range in a single measurement. The receiver measures the instantaneous value of the electric field itself, rather than the radiation intensity (electric field squared) as is typically done in optical spectroscopy. The frequency-dependent absorption coefficient and index of refraction of a given sample are obtained from the attenuation, delay, and distortion of the fs THz pulse transmitted through it. An additional advantage of this detection scheme is that it is performed coherently: the receiver is gated by a visible laser pulse in synchrony with the generation of the fs THz pulse, allowing a small signal to be detected amidst a large amount of thermal background black-body radiation.

There are several other techniques used to obtain information in this region of the spectrum, each with its own advantages and disadvantages. Microwave and FIR Fourier transform (FT-FIR) spectroscopies cover the spectrum from 1 to 10 cm^{-1} and 10 to 600 cm^{-1} respectively.^{9,10} Dispersive Fourier transform spectroscopy, in which the sample is placed only in one arm of the interferometer, allows measurement of both absorption and dispersion. This requires the assumption of perfect reflectivity for the interferometer mirrors over all wavelengths in the bandwidth of the light source. Because conventional radiation sources do not cover both microwave and FIR ranges, detailed studies of liquid dynamics have relied on a combination of these techniques.

[†] Presented at the Northeast Regional ACS Meeting in Rochester, NY (October 24 and 25, 1995), on the "Structure and Dynamics of Liquids".

[⊗] Abstract published in *Advance ACS Abstracts*, May 15, 1996.

A second method to measure spectra in the FIR utilizes line-tunable FIR lasers.¹¹ It is difficult to take spectra quickly at a variety of wavelengths with these sources since they are not tunable, and a different laser gas must be used for each wavelength. It is, however, possible to mix microwave frequencies with the fixed laser frequency to attain 4–10 cm⁻¹ of tunability around each laser line.¹² The scarcity of strong laser lines at low frequencies limits the spectral range of this technique to above 10 cm⁻¹. Typically, only absorption coefficients are measured with this technique, although in principle an interferometer can be used to determine the dispersion of the sample.

Line-tunable FIR radiation can also be achieved by difference frequency mixing two CO₂ lasers.¹³ By combining the output of CO₂ lasers with the various isotopes of C and O as well as with N₂O lasers, very good coverage is attained from 1 to 150 cm⁻¹.¹⁴ Further tunability is possible by mixing in microwave frequencies as well.¹³ A related development relies on difference frequency mixing two tunable diode lasers in a semiconductor device.¹⁵ The devices used are similar to those used to generate fs THz pulses, and tunable CW THz radiation between 0.1 and 3.8 THz has been demonstrated.¹⁵

Another light source used for FIR investigations of liquids is provided by synchrotron radiation.¹⁶ As is the case with the FIR lasers, an interferometer is required to measure the dispersion of the sample. A further limitation in this case is that synchrotron sources are not readily accessible. Finally, these sources also do not provide adequate coverage below 10 cm⁻¹.

Complementary to FIR spectroscopy in the investigation of liquid dynamics are studies that use visible laser light sources, such as low-frequency Raman scattering¹⁷ and optical-heterodyne-detected Raman-induced Kerr effect spectroscopy (OHD-RIKES).^{18,19} These techniques do not provide the linear dielectric properties of absorption and dispersion at FIR frequencies or the IR-active modes, but they do yield information regarding the intermolecular motions through the modulation of higher-order optical properties. Raman scattering¹⁷ has the advantage that it covers a broad spectrum, although at low frequencies it is limited to values greater than about 20 cm⁻¹ due to Rayleigh scattering. OHD-RIKES, which measures the decay of transient birefringence induced by an intense ultrashort laser pulse,^{18,19} provides the Raman spectrum over a wide spectral range, from 1 to 400 cm⁻¹. It requires that the laser pulse autocorrelation be deconvolved from the measured data and can suffer when the nonlinear response of the medium is dominated by electronic contributions, as is the case with water.¹⁹ The Raman techniques provide a normalized spectral density, whereas linear dielectric spectroscopy (i.e., FIR absorption and index of refraction) provides information specifically about the dynamics of molecular dipoles. While these two spectra will be very similar for small molecules, there could be significant differences for large molecules with polar groups.

The interpretation of low-frequency spectroscopic data from liquids has traditionally relied on a frequency separation between diffusive and resonant regimes. Resonant or oscillatory motion of a molecule (or group of molecules) can only be accommodated if the multidimensional potential energy surface sampled by the molecule is largely invariant over the time scale of multiple oscillations. Diffusive molecular motions, on the other hand, are those that occur slowly enough such that changes in the environment, rather than the inertia of the molecule, dictate their trajectory. Spectral features in the high-frequency, resonant region correspond to short-time recursions or oscillations in a time correlation function appropriate to a given technique, while the low-frequency, diffusive region yields

information about the “relaxation” or exponential decay of correlation at longer times. The onset of diffusive behavior is not necessarily well defined but expected to fall in the range 0.5–2 ps,¹⁹ suitable for probing by the 0.1–3 THz bandwidth of the fs THz spectrometer.

One of the strengths of using fs THz pulses is that they measure both the absorption and dispersion of the sample, allowing $\hat{\epsilon}(\omega)$ to be determined. The frequency-dependent, complex dielectric function, $\hat{\epsilon}(\omega) = \epsilon'(\omega) - \epsilon''(\omega)$, provides a fundamental description of a medium. In the diffusional regime, the frequency dependence of $\hat{\epsilon}(\omega)$ can often be successfully fit to analytic expressions based on bulk reorientational relaxation times, τ .²⁰

$$\hat{\epsilon}(\omega) = \epsilon_{\infty} + \sum_{j=1}^n \frac{\epsilon_j - \epsilon_{j+1}}{1 + (i\omega\tau_j)^{1-\alpha_j}\beta_j} \quad (1)$$

Here, ω is the angular frequency, ϵ_1 is the static dielectric constant, ϵ_j are intermediate steps in the dielectric constant, $\epsilon_{n+1} = \epsilon_{\infty}$ is its limiting value at high frequency, n is the number of relaxation processes, τ_j are their relaxation time constants, and α_j and β_j are parameters necessary for Cole–Cole or Cole–Davidson models, which describe a continuous distribution of relaxation times.

The Debye treatment with $n = 1$, $\alpha = 0$, and $\beta = 1$ is the simplest case. It requires that a single relaxation time provide an adequate description: in some sense, this indicates that all molecules sample the same environment over the time τ . The expression for $\hat{\epsilon}(\omega)$ from eq 1 simplifies to²⁰

$$\epsilon'(\omega) = \epsilon_{\infty} + \frac{\epsilon - \epsilon_{\infty}}{1 + i\omega\tau} \quad (2)$$

and it is easy to separate the real and imaginary components:²⁰

$$\epsilon'(\omega) = \epsilon_{\infty} + \frac{\epsilon - \epsilon_{\infty}}{1 + \omega^2\tau^2} \quad (3)$$

and

$$\epsilon''(\omega) = \frac{(\epsilon - \epsilon_{\infty})\omega\tau}{1 + \omega^2\tau^2} \quad (4)$$

More complicated models yield correspondingly more complicated expressions. Multiple Debye relaxation times are incorporated using eq 1 with $n > 1$, $\alpha = 0$, and $\beta = 1$. Some liquids exhibit a continuous distribution of relaxation times, which necessitates a Cole–Cole or Cole–Davidson description. A Cole–Cole treatment, with $0 < \alpha < 1$, describes a symmetric distribution about τ , while a Cole–Davidson treatment, with $0 < \beta < 1$, describes a skewed distribution. Both Cole–Cole and Cole–Davidson treatments can be applied to cases that have either a single distribution of times or multiple distributions ($n = 1$ or $n > 1$, respectively).

At higher frequencies, often on the order of 6 THz or greater, the response of dipolar liquids to oscillating fields is no longer overdamped but becomes resonant. Periodic motions, such as librations or translations within a solvent cage, are manifested as absorptions that are not associated with a monotonic decrease in the index of refraction. The presence of resonant bands will necessarily result in deviation from the dielectric relaxation models described above.

Finally, there has been much recent effort to describe liquids without the constraints imposed by analytical models by performing molecular dynamics (MD) simulations.^{21–23} The

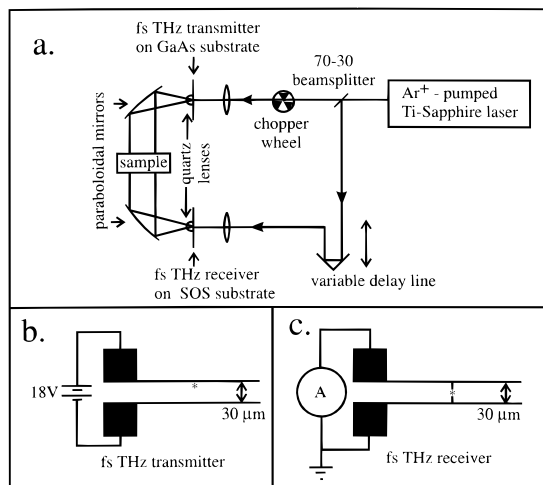


Figure 2. (a) Schematic diagram of fs THz transmission spectrometer. A fs THz pulse is generated at the transmitter when it is illuminated by a visible fs pulse from the Ti-sapphire laser. After collimation by the lens and paraboloidal mirror, the fs THz pulse passes through the sample and is refocused at the receiver. The receiver is gated synchronously by a portion of the beam split off from the visible pulse, so that the current flow at the receiver will map out the time-dependent electric field of the fs THz pulse as the variable delay is adjusted. (b, c) Schematic diagram of fs THz transmitter and receiver geometries. The asterisk represents the site at which the visible laser is focused.

interaction potential is specified, and a variety of observables can be determined. These models have successfully described the measured Stokes shift in time-resolved fluorescence Stokes shift (TRFSS) experiments, for example.²¹ The data presented in this paper determine $\hat{\epsilon}(\omega)$, and can be used as a test of the ability of MD simulations to determine equilibrium properties of polar liquids. While $\hat{\epsilon}(\omega)$ is a continuum description of a liquid, and not a molecular one, experimental measurements of it can be used to compare with the results of calculations based on molecular interactions. Some MD simulation methods, on the other hand, have incorporated $\hat{\epsilon}(\omega)$ to approximately account for long-range interactions at the time scale on which they occur.²⁴ Regardless of any specific theoretical treatment, experimentally determined values of $\epsilon'(\omega)$ and $\epsilon''(\omega)$ are essential for understanding the low-frequency dynamics of polar liquids.

Experimental Section

The method of generating and detecting fs THz pulses, based on that developed by several authors,¹ is shown schematically in Figure 2. A CW Ar⁺ laser (8–10 W) is used to pump a Ti-sapphire self-mode-locking femtosecond pulsed laser, which provides sub-80 fs pulses at 790 nm with approximately 12 nJ per pulse at 82 MHz (1 W average power). About 15% of the power is split off for pulse characterization and diagnostics. There are additional reflection losses from uncoated surfaces, resulting in roughly 700 mW of power available for fs THz pulse generation and detection. Two-thirds of the Ti-sapphire power is focused on the THz transmitter, and one-third of the Ti-sapphire power is used to operate the receiver. This is substantially higher than other workers have used,²⁵ but there were not any resultant signs of broadening of the fs THz pulse compared to lower power levels. It is possible that we were not focusing the visible beam as tightly as other workers do, thereby necessitating more visible power to generate the same intensity of visible light in the small active region of the devices (approximately 5 μm diameter).

The transmitter consists of a transmission line deposited lithographically on an undoped GaAs wafer. The parallel metal

strips of the transmission line are 1.6 cm in length and are separated by 30–60 μm. A dc bias voltage of 18 V is applied across the gap via wires bonded to pads at the end of each strip with indium metal. When a visible pulse from the Ti-sapphire laser illuminates the semiconductor surface between the metal strips, the acceleration of photoexcited electrons in the dc field radiates a fs THz pulse,²⁶ which is collimated by a crystalline quartz hyperhemispherical lens and an off-axis paraboloidal mirror. After passing through the sample, the pulse is refocused with a second mirror and lens combination onto the THz receiver, which is lithographically deposited on oxygen ion-implanted silicon-on-sapphire (O⁺ SOS).

The receiver structure is identical to the transmitter, except that an antenna with a 3–5 μm gap in the center bridges the transmission line. One-third of the Ti-sapphire beam is focused on this gap. The femtosecond visible beam causes a transient electrical short across the gap, allowing a current proportional to the instantaneous electric field to flow through the antenna. In order to determine the time-dependent electric field of the fs THz pulse, the relative delay between the generation of the fs THz pulse and the arrival of the visible gating pulse at the receiver is varied, and the electric field is measured at each time delay. The current that traverses the transiently shorted gap in the antenna is amplified with a lock-in amplifier referenced to a chopper that modulates the visible beam illuminating the transmitter. The transmitter, receiver, and beam path are all enclosed in a Plexiglas box which is purged with dry nitrogen to reduce absorption by atmospheric water vapor.

It is important to note that the spectral resolution of the spectrometer is dictated by the distance scanned by the optical delay line and is not limited by the short duration of the fs THz pulse.² In the present experimental setup, the response of the SOS receiver (including absorption by the sapphire substrate) dictates the upper limit of the useful frequency range; other workers have reported significant improvements in measured bandwidth upon switching to receivers with faster response characteristics.²⁷ The accurate measurement of linear optical constants, however, requires only that the receiver responds linearly at any given frequency and is independent of any additional knowledge of the frequency dependence of that response. In this study, although the data are collected in the time domain, we emphasize that we are utilizing the fs THz pulses merely as a broad-bandwidth FIR source with spectral components that have well-defined and easily measurable amplitudes and phases. The full capabilities of fs THz pulses for the study of liquids will be realized when they are used to obtain *transient* spectra in the FIR region of the spectrum.

Spectra of liquids at room temperature were measured with the use of a variable path length cell placed in the fs THz beam path. The liquid was sealed in a polyethylene bag and pressed between two parallel windows of either high-density polyethylene or high-resistivity silicon. One window was immobile, and the other was mounted on a translation stage. The path length could be varied with a precision of ±1 μm by adjusting the micrometer on the translation stage. The transmission of the THz pulse through the liquid in the sample cell was measured for several path lengths, at intervals of 50 or 100 μm, in the range of 50 to 1000 μm. At each path length, the time-dependent electric field of the transmitted fs THz pulse was obtained at 10 fs intervals over 10 ps by scanning the translation stage. Typically, 100 scans were averaged together, requiring a total acquisition time of roughly 5 min. The relative timing of the data points among a set of scans is known to within 6.67 fs (given by the 1 μm step size of the linear encoder on the optical delay line). A fast Fourier transform was applied to

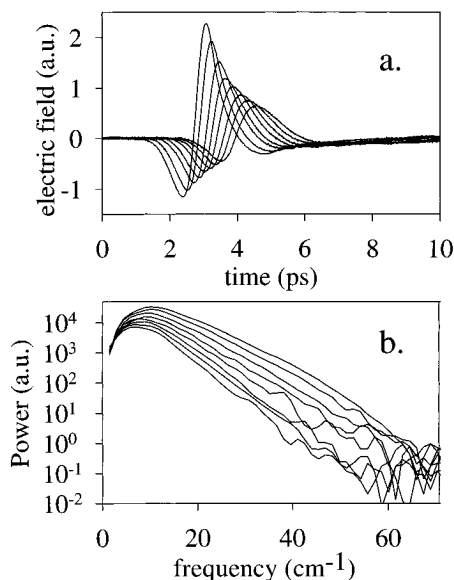


Figure 3. (a) Measured time profiles of the fs THz pulse transmitted through varying path lengths of ethanol over the range 200–900 μm ; the path length is increased by 100 μm for each scan. The pulse delay and attenuation increases as the path length increases. (b) Power transmission spectra derived from fast Fourier transform of the data in (a).

the time domain data, after subtracting a small linear base line term and zero-padding to obtain 2048 points, which then yielded the power $P(d, \nu)$ and phase $\phi(d, \nu)$ of each frequency component ν of the transmitted pulse for each path length d . As an example, the time domain transmission data and the corresponding power transmission spectra of ethanol for a range of path lengths are shown in Figure 3. The absorption coefficient at each frequency was determined by the slope of a linear regression fit of $\ln P(d, \nu)$ to path length, d :

$$\ln P(d, \nu) = \ln P_0(\nu) - \alpha(\nu)d \quad (5)$$

Similarly, the frequency-dependent index of refraction $n(\nu)$ was calculated from the path length dependence of the phases $\phi(d, \nu)$:

$$\phi(d, \nu) = \phi_0(\nu) + \frac{2\pi\nu(n(\nu) - 1)}{c}d \quad (6)$$

For each frequency, only those path lengths where $P(d, \nu)$ was greater than the noise level in the power spectrum by at least a factor of e (2.718), and where the single-pass attenuation of the pulse was greater than 50%, were included in the linear fits to reduce the influence of noise and etalon effects. With these restrictions, optical constants could be calculated from linear fits to data in the range 2–50 cm^{-1} .

Because the variable path length cell is not equipped for low-temperature operation, the spectrum of liquid ammonia was measured with fixed path length (100 and 200 μm) Infrasil quartz cells. Each cell was evacuated and then cooled by a flow of cold nitrogen gas through copper tubing coiled around the cell. Anhydrous ammonia gas was then allowed to condense directly into the cells. A stream of room-temperature nitrogen directed at the cell windows inhibited the formation of ice. The temperature inside the cells was estimated to be -40 $^{\circ}\text{C}$.

Results and Discussion

Figure 4 presents the frequency-dependent absorption coefficient for H_2O at room temperature measured by fs THz transmission spectroscopy over the range 2–60 cm^{-1} . The

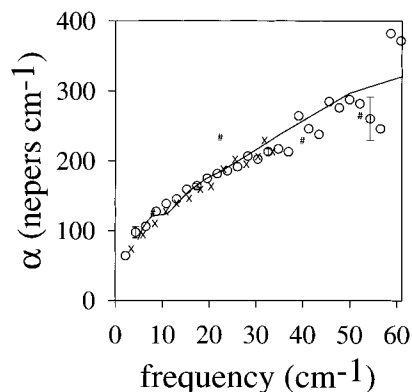


Figure 4. Power absorption spectrum of water at room temperature, with literature values for comparison: \circ , this study; solid line, FT-FIR results from Hasted et al.;²⁸ \times , fs THz pulse reflection results from Thrane et al.;⁷ #, FIR laser results from Vij et al.¹¹

results are in excellent agreement with previously reported spectra obtained by FT-FIR spectroscopy,²⁸ FIR laser spectroscopy,¹¹ and a reflection study using fs THz pulses.⁷ The transmission method employed here has several advantages over reflection methods: it allows convenient and accurate measurement of absorption for both strongly and weakly absorbing materials, it is simpler to implement as it does not require the fs THz beam to be split, and it does not rely on any knowledge of the optical constants of window materials. The primary disadvantage of the transmission method is that accurate analysis of strongly absorbing liquids requires data acquisition over a series of very short and precisely determined path lengths.

In this technique, primary data are collected in terms of the path length dependence of power attenuation $\alpha(\nu)$ and delay $n(\nu)$ of the fs THz pulse components as a function of frequency. While this is useful for describing the optical properties of a medium, it only provides limited insight into the liquid dynamics. In order to discuss dynamics, it is best to determine the frequency dependent complex dielectric constant, $\hat{\epsilon}(\omega)$. The frequency-dependent complex dielectric constant, $\hat{\epsilon}(\omega) = \epsilon'(\omega) - i\epsilon''(\omega)$, is related to the complex refractive index, $\hat{n}(\nu) = n(\nu) - ik(\nu)$, through the relations²⁹

$$\epsilon'(\omega) = n^2(\omega) - k^2(\omega) \quad (7)$$

and

$$\epsilon''(\omega) = 2n(\omega)k(\omega) \quad (8)$$

where $\omega = 2\pi\nu$ and $k(\omega) = \lambda\alpha(\omega)/4\pi = c\alpha(\omega)/2\omega$, with λ being the vacuum wavelength and c the speed of light in vacuum. Conversely, given $\epsilon'(\omega)$ and $\epsilon''(\omega)$, $n(\nu)$ and $\alpha(\nu)$ are seen to be

$$n(\nu) = \left(\frac{\sqrt{\epsilon'(2\pi\nu)^2 + \epsilon''(2\pi\nu)^2} + \epsilon'(2\pi\nu)}{2} \right)^{1/2} \quad (9)$$

$$\alpha(\nu) = \frac{4\pi\nu}{c} \left(\frac{\sqrt{\epsilon'(2\pi\nu)^2 + \epsilon''(2\pi\nu)^2} - \epsilon'(2\pi\nu)}{2} \right)^{1/2} \quad (10)$$

We have measured $n(\nu)$ and $\alpha(\nu)$ of water, methanol, ethanol, and 1-propanol in the range covering 3–34 cm^{-1} . Figures 5–8 present Cole–Cole plots [an Argand diagram of $\epsilon''(\omega)$ vs $-\epsilon'(\omega)$] as well as $n(\nu)$ and $\alpha(\nu)$ for these four liquids. Barthel et al.³⁰ previously derived relaxation parameters for these liquids based on data sets extending from 0.03 to 3 cm^{-1} for ethanol and 1-propanol, 0.03 to 10 cm^{-1} for methanol, and 0.03 to 14 cm^{-1} for water; $\alpha(\nu)$ calculated from their best fit parameters

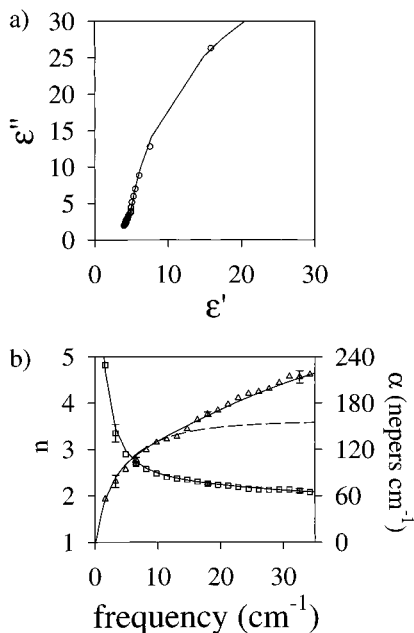


Figure 5. Comparison of experimental data for water to double Debye relaxation model. Solid lines are calculated from the parameters of Table 1. (a) Cole–Cole representation of the frequency-dependent complex permittivity. Open circles, data from this study. (b) Frequency-dependent power absorption coefficient (triangles) and index of refraction (squares). Dashed line is $\alpha(\nu)$ calculated with parameters from ref 30.

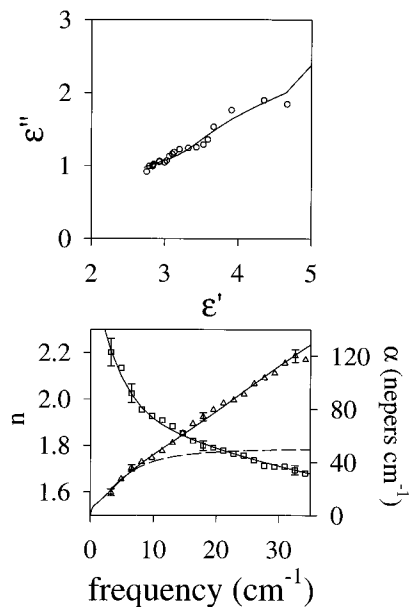


Figure 6. Comparison of experimental data for methanol to triple Debye relaxation model. Solid lines are calculated from the parameters of Table 1. (a) Cole–Cole graph of complex permittivity. (b) Power absorption coefficient (triangles) and index of refraction (squares). Dashed line is $\alpha(\nu)$ calculated with parameters from ref 30.

is shown as a dashed line in panel b of Figures 5–8. For each liquid, there is good agreement between our data and their best fits in the frequency range over which the two data sets overlap. In order to determine whether the marked deviation at higher frequencies was the result of the failure of the empirical dielectric relaxation theory or of the incompleteness of their data set, we fit the parameters ϵ_j and τ_j in eq 1 to our measured values of $n(\omega)$ and $k(\omega)$, using a nonlinear least-squares procedure. The parameters α and β were held fixed at 0 and 1, respectively, because the fit did not improve when they were varied. The fits, shown as solid lines in Figures 5–8, were constrained to be consistent with known dielectric behavior

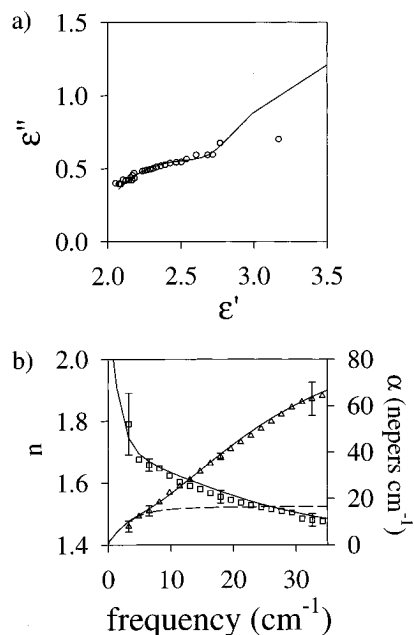


Figure 7. Comparison of experimental data for ethanol to triple Debye relaxation model. Solid lines are calculated from the parameters of Table 1. (a) Cole–Cole graph of complex permittivity. (b) Power absorption coefficient (triangles) and index of refraction (squares). Dashed line is $\alpha(\nu)$ calculated with parameters from ref 30.

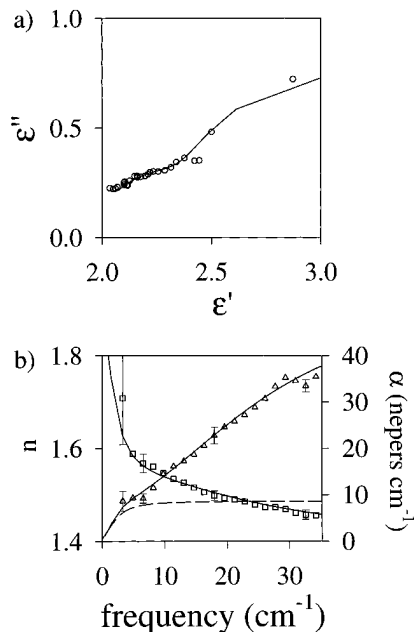


Figure 8. Comparison of experimental data for 1-propanol to triple Debye relaxation model. Solid lines are calculated from the parameters of Table 1. (a) Cole–Cole graph of complex permittivity. (b) Power absorption coefficient (triangles) and index of refraction (squares). Dashed line is $\alpha(\nu)$ calculated with parameters from ref 30.

below 3 cm^{-1} by inclusion of the static dielectric constant and data points in the range $0.03\text{--}1.43 \text{ cm}^{-1}$ based on the results of ref 30. Table 1 reports the results of the nonlinear least-squares fits, along with the parameters reported in ref 30 for comparison.

We found surprisingly good agreement between the measured data and the multiple relaxation model, even at higher frequencies where we expected that resonant absorption features would become important. For instance, we found a good fit with a double Debye model for H_2O , with $\tau_1 = 8.40 \text{ ps}$ and $\tau_2 = 0.19 \text{ ps}$. Barthel et al. fitted data up to 14 cm^{-1} with the same model and derived values of $\tau_1 = 8.32 \text{ ps}$ and $\tau_2 = 1.20 \text{ ps}$. The large

TABLE 1: Dielectric Relaxation Parameters of Water and Lower Alcohols, As Determined by Nonlinear Least-Squares Fit of the Data from This Study^a

liquid	ϵ_s	τ_1 (ps)	ϵ_2	τ_2 (ps)	ϵ_3	τ_3 (ps)	ϵ_∞
water	78.36 ^b [77.97]	8.24 (40) [8.32]	4.93 (54) [6.18]	0.18 (14) [1.02]			3.48 (70) [4.59]
methanol	32.63 ^b [32.50]	48 (4) [51.5]	5.35 (41) [5.91]	1.25 (55) [7.09]	3.37 (44) [4.90]	0.16 (11) [1.12]	2.10 (45) [2.79]
ethanol	24.35 ^b [24.32]	161 (21) [163]	4.15 (33) [4.49]	3.3 (1.3) [8.97]	2.72 (23) [3.82]	0.22 (09) [1.81]	1.93 (14) [2.69]
1-propanol	20.44 ^b [20.43]	316 (40) [329]	3.43 (21) [3.74]	2.9 (1.1) [15.1]	2.37 (15) [3.20]	0.20 (10) [2.40]	1.97 (12) [2.44]

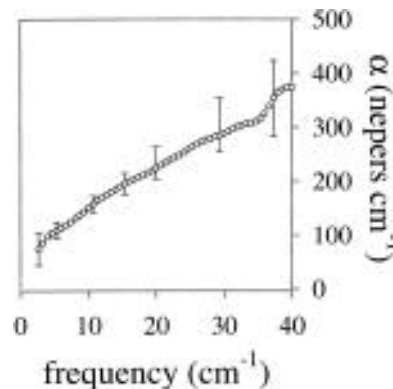
^a Values in parentheses are the 1σ uncertainties in the fitted parameters (expressed in units of the least significant digit reported). Values in square brackets are the parameters reported by Barthel et al. based on data extending to 409 GHz for water, 293 GHz for methanol, and 89 GHz for ethanol and 1-propanol.³⁰ ^b Literature values for static dielectric constants, taken from ref 30, were held constant during the least-squares fits.

discrepancy in τ_2 does not reflect an inherent shortcoming in the previous work, but rather their limited spectral range. The critical frequency for a Debye process with time constant τ is given by $\omega_{\text{crit}} = \tau^{-1}$. It corresponds to the frequency of maximum attenuation: $\epsilon''(\omega)$ has its maximum value and $\epsilon'(\omega)$ has an inflection point. If ω_{crit} is greater than the maximum probe frequency, it will be very difficult to accurately determine the Debye time constant. For the fastest process reported in Table 1 ($\tau_3 = 160$ fs for methanol), the critical frequency is 6.25×10^{12} rad/s, or 1 THz. Thus, it is seen that the fs THz pulses, with several THz of bandwidth, will be sensitive to even these fast processes, whereas 300 GHz microwave frequencies will not.

For the alcohols, we similarly found that extending the data set to 34 cm^{-1} led to a triple Debye model as previously obtained,³⁰ but again with significantly faster relaxation times for the second and third Debye processes. Dielectric relaxation models have traditionally been applied only at lower frequencies, based on the availability of $\hat{\epsilon}(\omega)$ and the assumption that faster processes will be oscillatory rather than diffusional. These new data show, however, that based on the dielectric properties alone there is no indication that 14 cm^{-1} rather than 35 cm^{-1} should be the frequency at which the Debye plateau for the second relaxation process in water begins. This highlights the importance of measuring the absorption and dispersion at high frequencies (up to 30 cm^{-1} or more), because otherwise the above assumption would remain untested.

An indication that a sufficient frequency range to completely describe the intermolecular dielectric relaxation has been achieved is the approach of ϵ_∞ to n_D^2 , where n_D is the index of refraction at 589 nm, the sodium D line. The square of the optical index of refraction, the electronic contribution to the dielectric constant, is a lower theoretical limit to ϵ_∞ .²⁰ In the alcohols, ϵ_∞ determined from this study is close (within the 1σ uncertainty of the fitted parameters) to n_D^2 , which lies near 1.8 for these four liquids. In water, however, the derived value of $\epsilon_\infty = 3.5 \pm 0.7$ is still significantly above the optical dielectric constant n_D^2 at 1.78, indicating that even higher-frequency processes contribute to intermolecular relaxation.

Although the data clearly fit the diffusional relaxation model of eq 1, the traditional interpretation of these very short relaxation times as representing an exponential, diffusive response is difficult to reconcile with the present understanding of the dynamics of polar liquids. It is known from time-resolved fluorescence Stokes shift experiments²¹ that rapid, inertial contributions to solvation account for up to 80% of the solvation process and are complete within 100–300 fs for small, polar solvents such as those considered here. Furthermore, the depolarized Raman³¹ and OHD-RIKES¹⁹ spectra of water show peaks at 60 cm^{-1} attributed to damped (but not diffusional) translational modes. The occurrence of inertial motions on the

**Figure 9.** Power absorption spectrum of liquid ammonia.

same time scale as τ violates the basic assumption of the diffusional model, namely, that relaxation dynamics occur on a time scale longer than that of inertial motion. Independent of any model, however, the determination of $\hat{\epsilon}(\omega)$ in the FIR region of the spectrum will allow a better test of continuum-based models of solvation, such as those based on the mean spherical approximation,³² which have had some success in accounting for time-resolved fluorescence Stokes shift results.²¹

Figure 9 displays the frequency-dependent absorption coefficient of liquid NH_3 . The sample temperature must be held below $-33 \text{ }^\circ\text{C}$, which prevents the variable path length sample cell from being used. Therefore, these optical constants have significantly more random and systematic error associated with them than those reported for the other liquids. The error bars shown represent the scatter of the data over measurements performed on different occasions with the two sample cells. The magnitude of systematic error associated with single path length measurement of absorption lies within the error bars shown. It is estimated by measuring the spectrum of H_2O in this quartz cell and comparing it to the known spectrum obtained with the variable path length cell. Systematic error in the dispersion spectrum, due to etalon effects in the empty cell, prevented the accurate measurement of the frequency-dependent index of refraction.

This is the first reported FIR spectrum of liquid NH_3 . The frequency dependence of absorption is similar to that observed in water. It is notable that NH_3 is more strongly absorbing in this frequency range than H_2O in spite of its lower dipole moment. This is probably due to a weaker hydrogen-bonding structure. One bond per molecule can be formed by ammonia, as opposed to two in water; furthermore, the structure of the liquid would be expected to be highly disrupted under the conditions of the experiment as the temperature was less than $10 \text{ }^\circ\text{C}$ below its boiling point. The absorption coefficient of H_2O in this region of the spectrum increases significantly as

the temperature is raised and can be estimated to be roughly 3 times larger at 85 °C than at room temperature.⁷

Conclusions

We have shown that fs THz pulses provide an efficient method to obtain the frequency-dependent absorption coefficient and index of refraction in the FIR region of the spectrum. This region bridges the gap between microwave techniques and standard FIR techniques and provides coverage in what has previously been a difficult region to work in. Dynamical information in both the diffusive and resonant regimes can be obtained because both absorption and dispersion are measured over a broad spectral range, although for the liquids studied here the onset of resonant absorption was not reached with the current bandwidth.

The results presented here show that simple dielectric relaxation models, which have long been known to describe dielectric behavior below 100 GHz, provide good fits to the experimentally determined complex dielectric constant of water and the lower alcohols up to at least 1 THz (33 cm⁻¹). The success of a diffusion-based model at such high frequencies is unexpected, but its validity is supported by the good agreement of model fits with both absorption and dispersion measurements. These results also underscore the importance of actually measuring the complex dielectric constant in the FIR region of the spectrum rather than using fitted parameters obtained at microwave frequencies to calculate it. The close approach of ϵ_∞ to n_D^2 for the alcohols suggests that complete dielectric relaxation is being observed; for water, however, this limit has not been achieved. The fastest relaxation times derived from this analysis are of the order 200 fs, 5 or more times faster than those reported previously. This result is relevant to studies of solvation, which often incorporate solvent dielectric relaxation times into the interpretation of time-resolved data. While the appropriate choice of model used to describe liquid dynamics in this frequency range is not always clear, an experimental determination of $\hat{\epsilon}(\omega)$ is a critical factor in the development and evaluation of models.

Finally, it is noted that fs THz pulses are ideally suited to probe picosecond and subpicosecond transient behavior in the FIR region of the spectrum. The generation and detection of the fs THz pulses can be synchronized with an event, such as a laser-induced excitation, to measure the THz spectrum at intervals following the event. In this way, one could directly monitor the evolution of the dynamic response of the medium.

Acknowledgment. The authors thank S. Ralph, D. Grischkowsky, P. Bucksbaum, and J. Whitaker for helpful discussions. We also thank J. Kessler for technical assistance. This work was partially supported by the Camille and Henry Dreyfus Foundation New Faculty Award Program and by a National Science Foundation Graduate Research Fellowship. Acknowledgment is made to the donors of the Petroleum Research Fund, administered by the ACS, for partial support of this research.

References and Notes

(1) Zhang, X.-C.; Hu, B. B.; Darrow, J. T.; Auston, D. H. *Appl. Phys. Lett.* **1990**, *56*, 1011. Katzenellenbogen, N.; Grischkowsky, D. *Appl. Phys. Lett.* **1991**, *58*, 222.

- (2) Harde, H.; Grischkowsky, D. *J. Opt. Soc. Am. B* **1991**, *8*, 1642. Harde, H.; Katzenellenbogen, N.; Grischkowsky, D. *J. Opt. Soc. Am. B* **1994**, *11*, 1018.
- (3) van Exter, M.; Grischkowsky, D. *Phys. Rev. B* **1990**, *41*, 12140.
- (4) Greene, B. I.; Saeta, P. N.; Dykaar, D. R.; Schmitt-Rink, S.; Chuang, S. L. *IEEE J. Quantum Electron.* **1992**, *28*, 2302.
- (5) Grischkowsky, D.; Keiding, S.; van Exter, M.; Fattinger, Ch. *J. Opt. Soc. Am. B* **1990**, *7*, 2006.
- (6) Pedersen, J. E.; Keiding, S. R. *IEEE J. Quantum Electron.* **1992**, *28*, 2518.
- (7) Thrane, L.; Jacobsen, R. H.; Uhd Jepsen, P.; Keiding, S. R. *Chem. Phys. Lett.* **1995**, *240*, 330.
- (8) Greene, B. I.; Federici, J. F.; Dykaar, D. R.; Levi, A. F. J.; Pfeiffer, L. *Opt. Lett.* **1991**, *16*, 48. Groeneveld, R. H. M.; Grischkowsky, D. *J. Opt. Soc. Am. B* **1994**, *11*, 2502.
- (9) Bell, R. J. *Introductory Fourier Transform Spectroscopy*; Academic: New York, 1972.
- (10) Czumaj, Z. *Mol. Phys.* **1990**, *69*, 787.
- (11) Vij, J. K.; Hufnagel, F. *Chem. Phys. Lett.* **1989**, *155*, 153.
- (12) Blake, G. A.; Laughlin, K. B.; Cohen, R. C.; Busarow, K. L.; Gwo, D. H.; Schmuttenmaer, C. A.; Steyert, D. W.; Saykally, R. *J. Rev. Sci. Instrum.* **1991**, *62*, 1701. Fetterman, H. R.; Tannenwald, P. E.; Clifton, B. J.; Fitzgerald, W. D.; Erickson, N. R. *Appl. Phys. Lett.* **1978**, *33*, 151.
- (13) Evenson, K. M.; Jennings, D. A.; Leopold, K. R.; Zink, L. R. In *Laser Spectroscopy VII. Papers from the Seventh International Conference on Laser Spectroscopy*; Hansch T. W., Shen, Y. R., Eds.; Springer: Berlin, 1985.
- (14) Blake, G. A.; Laughlin, K. B.; Cohen, R. C.; Busarow, K. L.; Gwo, D. H.; Schmuttenmaer, C. A.; Steyert, D. W.; Saykally, R. *J. Rev. Sci. Instrum.* **1991**, *62*, 1693.
- (15) Brown, E. R.; Mcintosh, K. A.; Nichols, K. B.; Dennis, C. L. *Appl. Phys. Lett.* **1995**, *66*, 285.
- (16) Dodo, T.; Sugawa, M.; Nonaka, E. *J. Chem. Phys.* **1993**, *98*, 5310. Fujita, Y.; Ohba, T.; Ikawa, S. I. *Can. J. Chem.* **1991**, *69*, 1745.
- (17) Versmold, H. In *Spectroscopy and Relaxation of Molecular Liquids*; Steele, D., Yarwood, J., Eds.; Elsevier: Amsterdam, 1991; pp 354–396.
- (18) McMorro, D.; Lotshaw, W. T.; Kenney-Wallace, G. A. *IEEE J. Quantum Electron.* **1988**, *24*, 443.
- (19) Castner, E. W.; Chang, Y. J.; Chu, Y. C.; Walrafen, G. E. *J. Chem. Phys.* **1995**, *102*, 653. Chang, Y. J.; Castner, E. W. *J. Chem. Phys.* **1993**, *99*, 7289.
- (20) Barthel, J.; Buchner, R. *Pure Appl. Chem.* **1991**, *63*, 1473.
- (21) Maroncelli, M. *J. Mol. Liq.* **1993**, *57*, 1. Maroncelli, M.; Fleming, G. R. *J. Chem. Phys.* **1988**, *89*, 875. Castner, E. W.; Maroncelli, M.; Fleming, G. R. *J. Chem. Phys.* **1987**, *86*, 1090.
- (22) Stratt, R. M.; Cho, M. *J. Chem. Phys.* **1994**, *100*, 6700.
- (23) Stassen, H.; Dorfmueller, T. *Chem. Phys.* **1994**, *187*, 337.
- (24) van Gunsteren, W. F.; Berendsen, H. J. C.; Rullmann, J. A. C. *Faraday Discuss. Chem. Soc.* **1978**, *66*, 58.
- (25) van Exter, M.; Grischkowsky, D. R. *IEEE Trans. Microwave Theory Tech.* **1990**, *38*, 1684.
- (26) Hu, B. B.; Weling, A. S.; Auston, D. H.; Kuznetsov, A. V.; Stanton, C. J. *Phys. Rev. B* **1994**, *49*, 2234.
- (27) Pedersen, J. E.; Keiding, S. R.; Sorensen, C. B.; Lindelof, P. E.; Rühle, W. W.; Zhou, X. Q. *J. Appl. Phys.* **1993**, *74*, 7022.
- (28) Hasted, J. B.; Husain, S. K.; Frescura, F. A. M.; Birch, J. R. *Chem. Phys. Lett.* **1985**, *118*, 622.
- (29) Birch, J. R.; Yarwood, J. In *Spectroscopy and Relaxation of Molecular Liquids*; Steele, D., Yarwood, J., Eds.; Elsevier: Amsterdam, 1991; pp 174–273.
- (30) Barthel, J.; Bachhuber, K.; Buchner, R.; Hetzenauer, H. *Chem. Phys. Lett.* **1990**, *165*, 369.
- (31) Mizoguchi, K.; Hori, Y.; Tominaga, Y. *J. Chem. Phys.* **1992**, *97*, 1961.
- (32) Wolynes, P. G. *J. Chem. Phys.* **1987**, *86*, 5133.